ACS OMEGA

Open Access

http://pubs.acs.org/journal/acsodf

Article

Simultaneous Effect of EBR on LLDPE and PDMS Rubber Blends and Its Nanocomposites for Cable Applications

Mostafizur Rahaman, Bibhudatta Paikaray, Mobasserul Islam, Subhadip Mondal, Jayakrushna Moharana, Saravanan Pandiaraj, Govindasami Periyasami, and Radhashyam Giri*

Cite This: *ACS Omega* 2024, 9, 828−836

Read Online

ACCESS | Metrics & More | Article Recommendations

ABSTRACT: The impact of electron beam radiation on the blend of linear low-density polyethylene (LLDPE) and polydimethylsiloxane (PDMS) rubber at different doses from 50 to 300 kGy has been investigated. The irradiated sheets were examined for their morphology, gel content, thermal stability, melt behavior, and electrical and dielectric properties. The radiation treatment has reduced both the melting point and crystallinity of base polymers and their blends because of chain scission. As observed, 100 kGy doses of irradiated blend and 3 wt % of loaded nanosilica composite showed comparatively good thermal stability. The phase morphology of the LLDPE: PDMS rubber blend showed a honeycomb-like design before irradiation because of two-stage morphology, which prominently changed into a solitary stage after electron beam irradiation. This is because of intermolecular cross-link arrangement inside the singular parts, just like cross-linking development at the interface. From the AQFESEM study, it is observed that the stacking of nanosilica particles within the blend matrix is greatly reduced after electron beam irradiation. The addition of nanosilica within the blend increased the electrical conductivity and dielectric permittivity. The dielectric breakdown strength has been observed to be the highest for 3 wt % loaded nanocomposite and its irradiated sample. The result indicates that the nanocomposite can be utilized for high-voltage cable applications in indoor and outdoor fields.

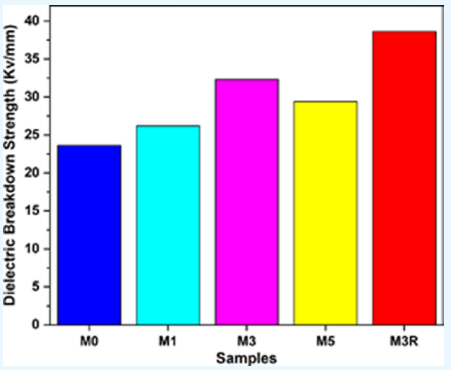

1. INTRODUCTION

Polydimethylsiloxane (PDMS), a hyperelastic material, is resistant to chemicals, biocompatible, transparent in nature, having gas permeability characteristics, thermally stable, and electrically insulators.[1] The hyperelastic and biocompatibility natures of this material allow it to be used for biomedical applications such as in microfluidic components,[2] bandages,[3] medical implants,[4] microvalves,[5] and in vitro diseases.[6] It is also used in microelectromechanical systems.[7] Because of high thermal stability and electrically insulating nature, it is used to protect components over a wider range of temperatures.[8] Silicone elastomers are generally thermosetting in nature. Hence, it is quite difficult to recycle it. However, there is a report of recycling PDMS where it was achieved through the reversible transesterification reaction.[9]

Polymers are cross-linked through either dynamic or radiation methods to get better properties. The irradiation method is advantageous and also interesting for the research community over the dynamic method because it is time-saving, can be performed at room temperature, is cost-effective, clean, can be controlled easily, is free from waste, no serious environmental hazard, is larger output, and can be applied to any geometrical shape and any stages of production.[10] Different radiation sources such as X-ray, gamma-ray, ultraviolet ray, and electron beam (EB) irradiation techniques are used to cross-link the polymers.[11] Among these sources, EB irradiation is more effective because of its high energy and penetrating power. Different doses of EB, applied on the test sample, result in different degrees of cross-linking. The radiation dose is expressed as Gray (Gy), which is defined as the dose required by 1 kg of material to absorb 1 Joule of energy. Accordingly, kGy stands for kilo Gray. Radiation exposure leads to chain scission and cross-linking in polymers and their blends by bringing about a 3-dimensional organization structure.[12] The degree of cross-linking depends on the intensity of the radiation dose. The expected results with irradiation cross-linking are that it may yield polymeric materials with improved dimensional stability, reduced stress cracking, higher service temperature, reduced solvent, and water permeability, contributing significantly to the improvement in some thermomechanical characteristics, improvements

Received: September 7, 2023
Revised: November 22, 2023
Accepted: December 13, 2023
Published: December 22, 2023

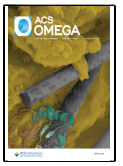

of tensile strength, elongation at break and heat deformation, and decrease of thermal expansion of the blends.[10,13]

This irradiation process has been used in the power cable industry and is distinguished as the most developed industrial process. Many analysts have detailed the behavior of polymers and polymer blends when they are exposed to EB radiation (EBR). For example, an upgrade in the properties of the PVC-ENR blend could be accomplished by pre-irradiating the rubber after melt blending. A sufficient increase in impact strength compared with tensile strength implied that the cross-linking of the rubber phase in the PVC-ENR blend played an important role in resisting crack propagation during the impact test.[14] In another study, authors prepared the blend of polypropylene/ethylene-propylene-diene monomer (PP/EPDM) and initiated cross-linking in the dispersed EPDM phase by EBR that brought about the stabilization of the phase morphology.[15] Physicomechanical properties of waste polyethylene (WPE) and WPE/low-density polyethylene (LDPE) (70/30)-based blend were increased with an increment in cross-link density.[16] The compatibility, physicomechanical properties, and structure−property relationship of LLDPE, PDMS, and their blends were studied at different radiation dosages.[17]

LLDPE/PDMS-based blend nanocomposites, filled with boron nitride (BN), were studied to check their applicability for a high-voltage insulator.[18] The composites were prepared in three different manners: First, BN was added with LLDPE and PDMS directly; second, BN was master-batched with PDMS and then added with LLDPE; and third, BN was master-batched with LLDPE and then added with PDMS. Results showed that the addition of BN improved the dielectric constant, loss, and breakdown strength of the nanocomposites. Moreover, the PDMS-BN master-batched nanocomposite exhibited low dielectric constant and loss but high breakdown strength compared with the other two nanocomposites. Said et al. have reported the effects of different nanofillers on the dielectric insulating performance of cross-linked polyethylene (XLPE).[19] They have used silica, titania, and zinc oxide as nanofillers with varying compositions and prepared their composites by a melt blending process. The nanofillers were surface-modified. They have reported that the melting point of functionalized XLPE/TiO_2 nanocomposite had increased by 6.85 °C compared to neat XLPE; whereas, silica-filled nanocomposite showed more improvement in dielectric properties. There is plenty of literature discussing the polymer, polymer blends, and polymer-based composites used in high-voltage cable applications.[20] However, the work on high-voltage cable application of LLDPE/PDMS blend-based nanosilica nanocomposite cured by electron beam irradiation is really scanty.

Hence, the goal of the current work is to prepare EB-irradiated LLDPE/PDMS blend-based nanosilica nanocomposites and investigate their suitability to be used for high-voltage cable applications. Accordingly, we have tested the thermal, electrical, and dielectric properties, and morphology of the nanocomposites. We have investigated the melting behavior, crystallinity, thermal stability, electrical resistivity, dielectric permittivity, and most importantly, the dielectric breakdown strength, which will provide the nanocomposites' suitability to be used for high-voltage cable application.

2. MATERIALS, METHODS, AND EXPERIMENTS

2.1. Materials Used. LLDPE (grade RELENE E 24065) has been provided by Reliance Industries Ltd., India. Its physical characteristics such as melt flow index (MFI), melting point, and density are 6.5 g/10 min, 122 °C, and 0.924 g/cm^3, respectively. PDMS rubber (Silastic WC-50), having a density of 1.15 g/cm^3 at 25 °C, has been obtained from Dow Corning Inc., USA. Ethylene methyl acrylate (EMA) copolymer resin (OPTEMA TC-120), containing 21% methyl acrylate, has a melting point of 81 °C, a density of 0.94 g/cm^3, and MFI of 6.0 g/10 min, and has been provided by Exxon Chemicals Eastern Inc., Mumbai, India. Nanosilica (molecule size ∼5−15 nm) was obtained from Aldrich Chemical Co. Ltd., USA. Toluene and xylene, utilized as solvents, were produced by Merck Specialties Private Limited, Mumbai, India.

2.2. Blends and Test Specimen Preparation. The blending of PDMS and LLDPE was performed at their different proportions within an internal blender (Haake Rheomix, Model: Rheomix 600 OS, Thermo Fisher Scientific, Massachusetts, USA). The blending was done at the rotor speed of 100 rpm and temperature of 200 °C for 8 min. The chamber was first filled with LLDPE, which was allowed to melt for a few seconds before the PDMS rubber was added. For the preparation of ternary blend composites, the PDMS rubber and EMA were melt-mixed first for 4 min using the same instrument at the same temperature of 200 °C and rotor speed of 100 rpm, and then LLDPE was added to it. This was mixed for another 4 min and last a required quantity of nanosilica was added within it and the mixing was further continued for an additional 4 min according to the composition given in Table 1. On a two-roll open mill, the molten mass was sheeted out at room temperature. After that, they were molded into sheets with dimensions of 14 cm × 1.5 mm × 2 mm in a compression molding hydraulic press (Model: SKU-A80415.01, George E. Moore and Son Press, Durham, UK) for two min at a temperature of 200 °C and a

Table 1. PDMS, LLDPE, and Their Blends before and after Compatibilization with Variations in Nanosilica as well as Radiation Doses

sample code	LLDPE (wt %)	PDMS (wt %)	EMA (wt %)	nanosilica (wt %) + 10% Si69 with respect to silica	radiation dose (kGy)
LL100	100	0	0	0	0
$LL100R_{50}$	100	0	0	0	50
$LL100R_{100}$	100	0	0	0	100
$LL100R_{150}$	100	0	0	0	150
LL50	50	50	0	0	0
$LL50R_{50}$	50	50	0	0	50
$LL50R_{100}$	50	50	0	0	100
$LL50R_{150}$	50	50	0	0	150
PD100	0	100	0	0	0
$PD100R_{50}$	0	100	0	0	50
$PD100R_{100}$	0	100	0	0	100
$PD100R_{150}$	0	100	0	0	150
M_0	50	50	12	0	0
M_1	50	50	12	1	0
M_3	50	50	12	3	0
M_5	50	50	12	5	0
M_3R	50	50	12	5	100

https://doi.org/10.1021/acsomega.3c06766
ACS Omega 2024, 9, 828−836

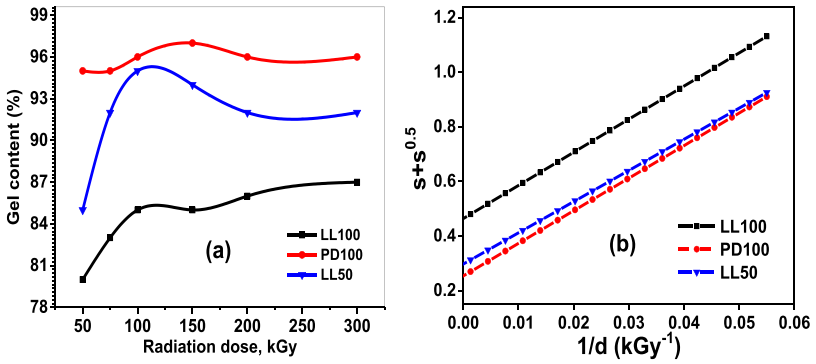

Figure 1. (a) Gel content, %, of LL100, PD100, and their blend before and after electron beam irradiation and (b) plot of $(s + s^{0.5})$ versus $1/d$ (kGy^{-1}) for LL100, PD100, and their blend.

pressure of 5 MPa. By passing cold water through the platens, the mold was brought down to room temperature.

2.3. Irradiation of the Composite Samples. The EB irradiation of the samples was performed at the Bhabha Atomic Research Centre (BARC), Bombay, India. In this process, the samples in sheet form were irradiated by using an accelerator (ILU Machine, Model: ILU-6, Budker Institute of Nuclear Physics, Novosibirsk, Russia), having beam power 5 W/mm^2 with adjustable beam window of dimension 950 mm × 70 mm. The EB was generated in a LaB_6-made cathode by using a radio frequency generator. During the measurement, the electron beam was accelerated at a high frequency within electromagnetic field keeping toroidal resonator under vacuum 10^{-6} Torr. The samples were irradiated at normal temperature by an air-cooling process where the speed of conveyor belt was 0.9 m/min. The beam current and accelerated energy utilized were 1 mA and 1.8 MeV, respectively.

2.4. Experiments. The gel content of the test samples has been characterized as per ASTM D 2765. We have determined the melting behavior and thermal stability of some selected samples by using instruments such as differential scanning calorimetry (DSC) and thermogravimetric analysis (TGA), respectively. The DSC study was performed by utilizing a TA Instruments (DSC Q 100 thermal analyzer, New Castle, Delaware, USA) at the ramp at 10 °C/min under a nitrogen environment within the temperature range −130 to 160 °C. The TGA of pure components, their blends, and blend nanocomposites before and after FB irradiation was estimated by utilizing the instrument TG Q50 (Q50 V6.1 series, TA Instruments, New Castle, Delaware, USA) under nitrogen atmosphere at the ramp 20 °C/min from the temperature 30 to 700 °C. The etched surfaces of the pre- and post-EB-irradiated samples were examined using a scanning electron microscope (SEM; Model: JEOL JSM-5800, Tokyo, Japan) to check their phase morphology. The morphology of specimens was also analyzed by a high-resolution transmission electron microscope (HRTEM, JEM 2100, JEOL Limited, Tokyo, Japan). For TEM analysis, the specimens were dried overnight in a vacuum oven. Then, the specimens were cut into ∼50 nm-thick segments on a LEICA ULTRACUT UCT (Leica Microsystems GmbH, Vienna, Austria) microtome equipped with a diamond knife having a cutting edge of 45°. The preparation of the section was conducted at 0.001 m/s at −50 °C in a liquid nitrogen environment. A high resistance meter (Model: Agilent 4339B, Agilent Technologies, California, USA) was used to test the samples' electrical volume resistivity (dimension 10 × 10 cm^2) at room temperature, in accordance with ASTM D-257-66. The impedance spectra, dielectric permittivity, and dielectric loss of the samples with thickness ∼0.22 mm were measured over the frequency range $10-10^6$ Hz by utilizing a dielectric analyzer (Model: DEA 2970, TA Instruments, New Castle, Delaware, USA) interfaced with a controller 2000 as per ASTM D 150. The dielectric breakdown strength of the samples was tested as per ASTM D149.87 by utilizing a breakdown voltage tester at 100 Hz (Model: KP8009, KEPIN Fire Testing Technology Ltd., Dongguan, China). The thickness of the samples was ∼0.2 mm.

3. RESULTS AND DISCUSSION

3.1. Gel Content Analysis. The percent gel content of LLDPE, PDMS rubber, and their blend are plotted against the irradiation dose in Figure 1a. It is observed from the figure that the gel content is consistently increasing with an increase in radiation dosage for neat LLDPE but for its blend, it has increased up to radiation of 100 kGy, and then the gel content has reduced for the blend, and PDMS rubber up to the highest radiation dose of measurement. The drastic drop in the gel content beyond 100 kGy in the case of LL50 is possibly due to a competition between PDMS rubber and LLDPE for forming the cross-linked network as one has (LLDPE) slower response to radiation than the other (PDMS), which responses quickly to radiation forming cross-linking network structure. The sol fraction (s) of a radiated cross-linked polymer can be correlated to the inverse of the irradiation dose as per the Charlesby−Pinner equation:[21]

$$s + \sqrt{s} = \frac{p_0}{q_0} + \frac{10}{q_0 \mu d} \quad (1)$$

where μ is the number-average degree of polymerization, q_0 is the density of cross-linked units per unit dose (kGy^{-1}), p_0 is the fracture density per unit dose (kGy^{-1}), and d is the radiation dose (kGy). This gives an idea of the ratio of chain scission to cross-linking for the pure polymers exposed to irradiation. But, in LLDPE, PDMS, and their blend give a linear relationship between $(s + s^{0.5})$ and $1/d$ as expected from the Charlesby−Pinner equation shown in Figure 1b. The p_0/q_0 ratio (intercept of the straight line in the plot) for PDMS, LL50, and LL100 is 0.25, 0.30, and 0.46, respectively. The radiation exposure of the LLDPE, PDMS, and their blend lead to cross-linking, which follows the order LL100 < LL50 < PDMS. In this way, there is a competition between cross-link arrangement and chain scission in the polymer blend matrix. However, the cross-linking reaction predominates the chain

https://doi.org/10.1021/acsomega.3c06766
ACS Omega 2024, 9, 828−836

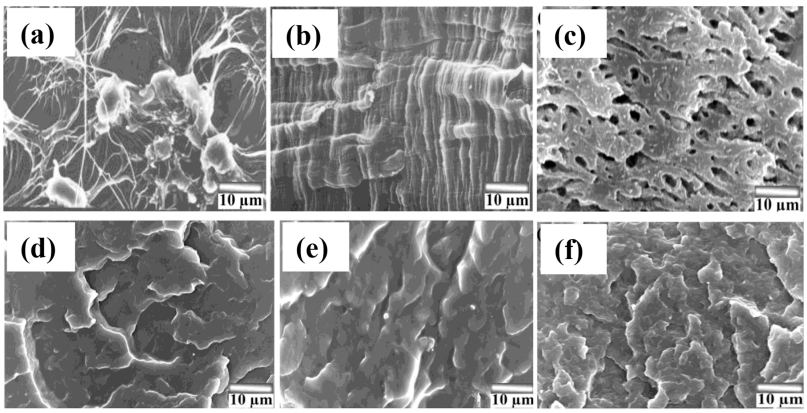

Figure 2. SEM photographs of (a) LL100, (b) PD100, (c) LL50 before electron beam irradiation and (d) LL100, (e) PD100, and (f) LL50 after electron beam irradiation at 100 kGy.

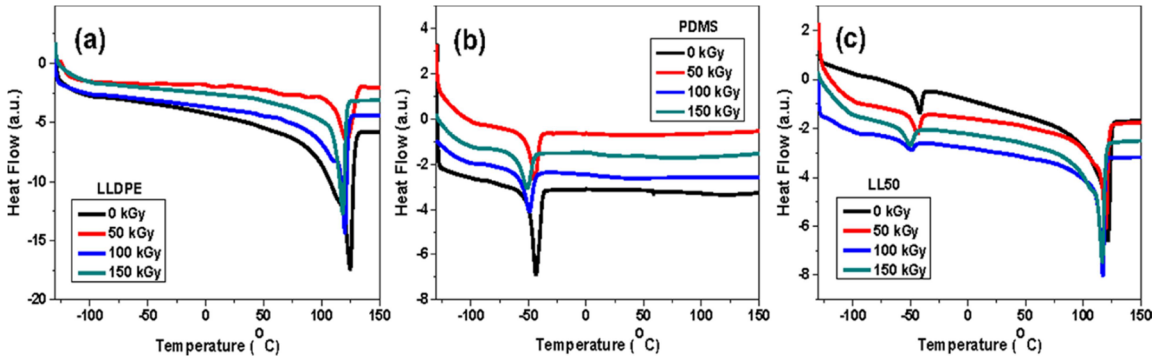

Figure 3. DSC plots of (a) LL100, (b) PD100, and (c) LL50 with the variation of irradiation dose.

Table 2. Extracted Data from DSC Thermogram

					LL50			
	LLDPE		PDMS		LLDPE		PDMS	
radiation doses	T_m	%Xc	T_m	%Xc	T_m	%Xc	T_m	%Xc
0 kGy	124.5	52.6	−43.3	36.4	121.5	44.6	−42.3	28.4
50 kGy	121.6	51.2	−44.3	32.3	119.8	42.3	−43.9	26.8
100 kGy	120.2	49.3	−49.2	31.5	117.1	39.5	−48.3	23.9
150 kGy	118.2	42.4	−51.4	29.8	116.6	37.2	−50.2	21.3

scission/degradation over lower doses of irradiation and the reverse trend is observed over higher doses.

3.2. Scanning Electron Microscopy. The phase morphology of LLDPE, PDMS, and LL50 blend before and after irradiation has been studied by scanning electron microscopy after cryo-fracturing and etching the surfaces in toluene and sputter coating the dried surface with gold. Figure 2a shows the SEM photomicrograph of the neat LLDPE, which exhibits the flower-like crystals of LLDPE generated during the cryo-fracture of samples. It shows a few fibrous structures. The SEM photomicrograph of the cry-fractured sample of neat PDMS is shown in Figure 2b. It shows systematic flow lines indicative of ductile failure. Similarly, a photomicrograph in Figure 2c of the LL50 blend before irradiation exhibits more undulations and an intense honeycomb structure due to a higher proportion of silicone rubber domains driven out of the blend. It clearly shows that the silicone rubber domains in the micrometer scale were dispersed within the LLDPE matrix and acted as a co-continuous phase. After irradiation at 100 kGy, the fracture surface of LLDPE does not show the fibrillar structure and flowers of crystals but shows a ductile failure with a large flow path as shown in Figure 2d. Similarly, Figure 2e shows a ductile failure for a neat PDMS matrix. Figure 2f shows the SEM photograph of the LL50 blend irradiated at 100 kGy after etching in toluene to extract the silicone rubber phase if left uncross-linked. However, on cross-linking by electron beam irradiation, the silicone rubber phases were attached to the LLDPE matrix at the interface, and no etching was possible. It exhibits a single-phase morphology, with the orientation of the matrix in one direction simulating the flow lines.

3.3. DSC Studies. The melting and crystallization behaviors of neat LLDPE, neat PDMS, and their blends with varying irradiation doses are shown in Figure 3a−c. The extracted values of the melting point (T_m) and percent crystallinity (%Xc) are presented in Table 2. Figure 3a presents the DSC thermograms of neat LLDPE irradiated at different doses. The figure shows a significant change in the size and shape of the melting peak. Figure 3b shows the brittleness temperature of the PDMS rubber before and after irradiation at

https://doi.org/10.1021/acsomega.3c06766
ACS Omega 2024, 9, 828−836

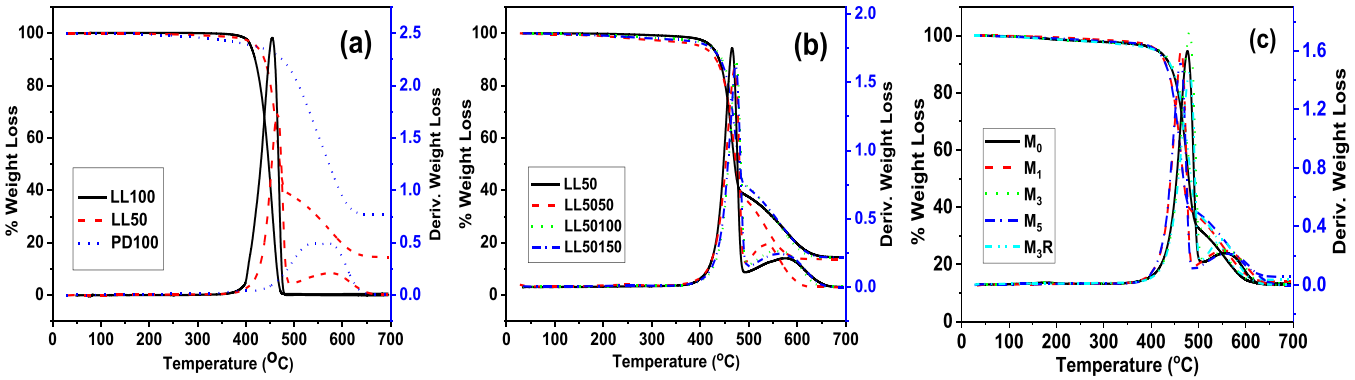

Figure 4. (a) TGA of LLDPE, PDMS, and their blend, (b) TGA of LL50 with the variation of irradiation dose, and (c) TGA of LL50 blend nanocomposites.

various doses. The DSC results also supported that the increase in the radiation dose brought about a reduction in the level of percent crystallinity (Xc), which likewise reflects in the decrease of melting temperature (T_m). This is attributed to the formation of a 3D network, which inclines toward clearly lamellar thickening during crystallization and results in the reduction of melting temperature. In the case of PDMS, the endothermic peak at −43.3 °C corresponds to the brittleness temperature that is the cold crystallization of PDMS. For the blend of LLDPE-PDMS rubber, DSC thermograms display two different endothermic peaks around 121.5 and −44.6 °C, as displayed in Figure 3c. The extremely sharp peak at 121.5 °C corresponds to the melting point of LLDPE, whereas the less prominent peak around 44.6 °C corresponds to the brittleness point of PDMS. The existence of two separate peaks for the LL50 blend indicates that the two polymers are incompatible in their blend system. It is envisaged from the figure that for the LL50 blend, the endothermic peak areas have decreased and shifted marginally toward lower temperatures corresponding to the melting of LLDPE with the increase in the irradiation dose. However, the melting points corresponding to PDMS have shifted slightly to higher temperatures as shown in the table.

3.4. Thermogravimetric Analysis. The TGA and derivative TGA plots of neat LLDPE, neat PDMS, their blends, and nanocomposites are displayed in Figure 4a−c. The extracted data from TGA and derivative TGA plots of the start of thermal decomposition (T_i), degradation maxima (T_{max}) due to LLDPE and PDMS, degradation temperature at 50% weight loss (T_{50}), and residue at 680 °C are presented in Table 3. The initiation of thermal decomposition (T_i) has been considered at 5% decomposition for the polymers, their blend, and nanofilled composites. Accordingly, T_i for neat LLDPE (LL100) occurs at 410.0 °C. When the temperature is further raised, there is the formation of free radicals because of the degradation and breakdown of the covalent C−C bonds. On the contrary, neat PDMS exhibited T_i at 419 °C. It is because of the high −Si−O− bond energy present in PDMS. On the other hand, the LL50 blend shows a marginal improvement in the T_i value that is around 423 °C compared to neat LLDPE's T_i value of 410 °C. The thermal stability (T_{max}) for LLDPE and PDMS are 454 and 554 °C, respectively. However, in their blend, the T_{max} value for both LLDPE and PDMS parts has increased to 465 and 590 °C, respectively. The percentage residues are higher for PDMS and PDMS-filled blends. After EB irradiation, LL50 shows improvement in thermal stability in its LLDPE part, which is around 474 °C at an irradiation dose of 100 kGy shown in Figure 4b. Among the nanosilica-loaded nanocomposites, M_3 showed the highest thermal stability. Again, the thermal stability slightly increased after EB irradiation of the optimum nanosilica-loaded nanocomposite.

Table 3. TGA Data of LLDPE, PDMS, Their blends, and Nanocomposites

		T_{max} (°C)			
sample code	T_i (°C)	LLDPE	PDMS	T_{50} (°C)	% residue @680 °C
LL100	410	454		447	0.51
LL50	423	465	590	471	14.5
PD100	419		554	572	30.6
LL5050	401	470	535	473	13.7
LL50100	422	474	557	480	14.4
LL50150	417	472	561	479	14.4
M_0	411	477	556	479	13.3
M_1	412	464	555	468	14.0
M_3	415	480	561	483	13.4
M_5	411	462	559	468	15.6
M_3R	407	481	549	484	14.5

3.5. Morphological Analysis of Nanocomposites through HRTEM and FESEM. To examine the state of dispersion of silica nanoparticles in the bicomponent polymeric matrix, a TEM analysis was performed for some selected samples. The TEM photomicrographs of these selected samples are displayed in Figure 5. All samples were stained with osmium tetroxide before testing and accordingly given higher scattering cross sections to incident electrons. The dispersion of nanosilica in the blend matrix is found to be good for all nanocomposites except for the M_5 sample as seen from the TEM images displayed in Figure 5. Hence, the sample M_5 shows inferior thermal properties compared to the M_3 sample. This is why the optimum loading of nanosilica was chosen as 3 wt %, which enhanced the thermal properties of the LLDPE-PDMS rubber blend system. The sample M3R also showed good dispersion of nanosilica particles within its polymer matrix. The FESEM study of similar samples is presented in Figure 6. It is observed that the stacking of nanosilica particles in the blend matrix is greatly reduced due to the electron beam irradiation, as shown in Figure 6d.

3.6. Electrical Properties. The DC resistivity of the blend LLDPE + PDMS + EMA system, its nanosilica-loaded composites, and the radiation doses optimized sample are presented in Figure 7. The figure shows that the electrical

https://doi.org/10.1021/acsomega.3c06766
ACS Omega 2024, 9, 828−836

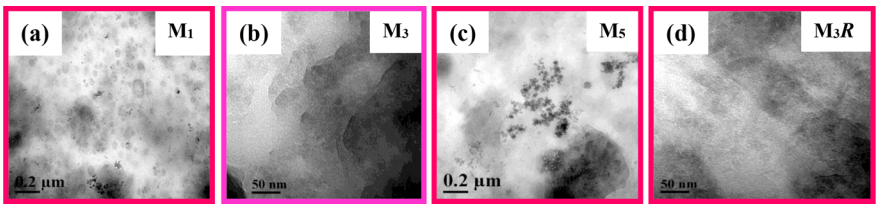

Figure 5. TEM photomicrographs of the samples (a) 1%, (b) 3%, (c) 5% nanosilica in compatibilized blend nanocomposites before EBR, and (d) 3% nanosilica in compatibilized blend nanocomposites after EBR at 100 kGy.

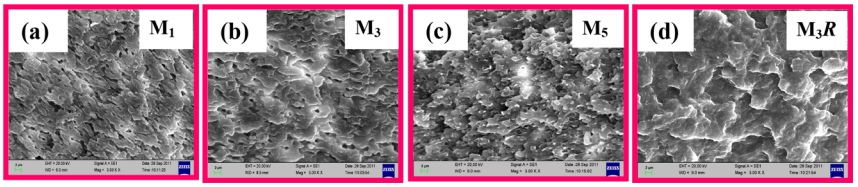

Figure 6. FESEM photomicrographs of the samples (a) 1%, (b) 3%, (c) 5% nanosilica in compatibilized blend nanocomposites before EBR, and (d) 3% nanosilica in compatibilized blend nanocomposites after EBR at 100 kGy.

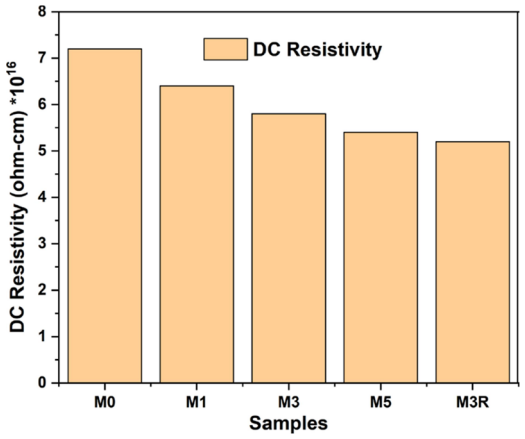

Figure 7. DC resistivity of nanosilica-filled nanocomposites.

resistivity has reduced after the addition of nanosilica within the blend system. The results indicate that the resistivity of all composites falls within the insulating range. Therefore, the composites behave as insulators. There is no material, which behaves like a perfect insulator that means no conduction of charge carrier. Insulators also possess some mobile charge carriers, which are responsible for their very low electrical conductivity. For our samples, the order of electrical resistivity is 10^{16} ohm-cm. With the progressive increase in nanosilica loading within the blend system, the resistivity has also been reduced gradually. For the M5 composite, there is a 26.7% decrement in electrical resistivity compared to the nanosilicaless M0 blend. Nanosilica consists of silanol (hydroxyl) groups (Si−OH) on its surfaces that are responsible for its polarity in nature.[22] When an external electric field is applied to the composite materials, then this internal polarity becomes in order, which in turn increases the mobility of charge carriers and results in a decrease in electrical resistivity.[23] It is observed from the figure that the radiation-cured sample (M3R) shows less electrical resistivity compared with the nonradiated one (M3) or nanosilicaless M0 blend. The curing of polymers makes them more compact within the composite system and brings the nanosilica particles closer to each other. As a result, the mobility of charge carriers gets facilitated and leads to a lower value of electrical resistivity.[24]

The log−log plots of impedance spectra of the composites versus frequency are presented in Figure 8. The impedance

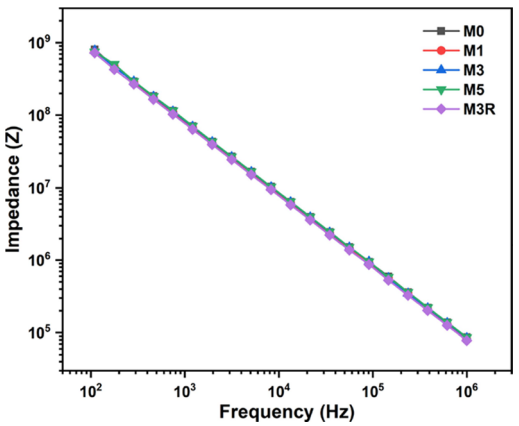

Figure 8. Impedance spectra of nanosilica-filled nanocomposites.

values show frequency-dependent behavior, that is, the impedance values decrease linearly with the increase in the frequency of the electric field. At a frequency of 10 Hz, the value of impedance is approximately 10^9 ohms, which has reduced to below 10^5 ohms at the frequency of 10^6 Hz. Hence, the impedance value has reduced at the order of 10.[4] The patterns of all curves are almost identical. There is no substantial reduction of impedance value with the increase in silica loading as well as radiation curing, indicating that the charge carrier density has not improved too much after the addition of silica and curing of the samples. However, the increased frequency has impacted drastic improvement in charge carrier density: as a result, the impedance has reduced several orders of magnitude.

3.7. Dielectric Properties. The dielectric constant, dielectric loss, and electric modulus of the nanocomposites both with respect to frequency and silica loading are presented in Figure 9. It is observed from Figure 9a that the dielectric constant value decreases with the increase in frequency but increases with the increase in silica loading. The decrement in dielectric constant value over the low-frequency range is more compared to the decrement over high frequencies. Over lower frequencies, the dipoles get more time to relax/orient

https://doi.org/10.1021/acsomega.3c06766
ACS Omega 2024, 9, 828−836

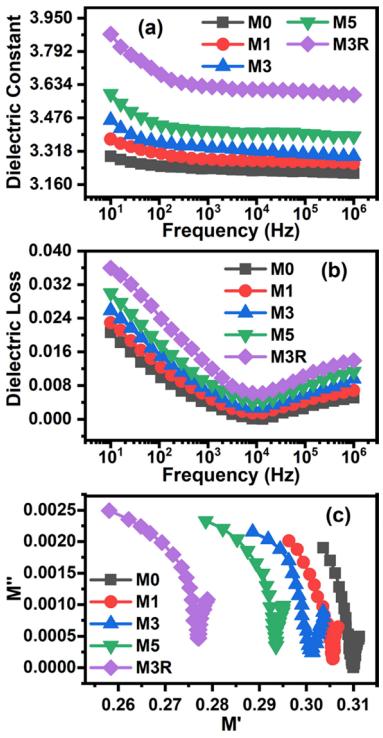

Figure 9. (a) Dielectric constant, (b) dielectric loss, and (c) electric modulus of nanosilica-filled nanocomposites.

themselves toward the direction of the applied AC electric field. As a result, the magnitude of orientation toward the direction of the applied electric field becomes greater over lower frequencies compared to the orientation effect over higher frequencies. This is why the dielectric constant value over the lower frequencies shows a high value for all composites compared to higher frequencies. It is observed from the figure that the trend in the decrement of dielectric constant over lower frequencies is exponential in nature, whereas, over higher frequencies, this decrement trend is almost linear. This high change in the dielectric constant value over lower frequencies may be because of the effect of interface polarization. With the increase in frequency, this effect of interface polarization is gradually diminished and results in less decrement of dielectric constant value.[25] It has been mentioned earlier that the dielectric constant value is increasing with the increase in nanosilica loading within the polymer matrix when considering any particular frequency. This increment in dielectric constant value is because of the presence of a polar silanol group on the surface of nanosilica. These polar groups orient themselves toward the applied electric field and contribute to the increase in dielectric constant value.[26,27] Moreover, there is also the effect of interface polarization generated between polymer−polymer, filler−filler, and polymer−filler interfaces, which increases the dielectric constant value. With the increase in nanosilica loading, the filler−filler and polymer−filler interface polarizations increase, and hence, a gradual increase in dielectric constant value is observed. The cured sample (M3R) shows the highest value of the dielectric constant over the whole frequency range. Actually, the curing of the sample has made the polymer composite more compact as stated earlier. As a result, the dipoles come closer to each other, which leads to a higher effect of interface polarization compared with uncured ones and thus increases the dielectric constant value.

The effects of frequency and nanosilica loading on the dielectric loss value are shown in Figure 9b. It is observed that unlike the dielectric constant, the dielectric loss value has decreased initially up to a certain frequency and then has increased up to the highest frequency level of measurement. The application of electric field results in the orientation of dipoles toward the applied field. This orientation is compensated by the loss of energy. Moreover, because of polarization at the interface, there is also the loss of energy. As the effects of orientation and interface polarization are more over low frequency, the dielectric loss is also high. With the increase in frequency, both the effects are reducing; as a result, the dielectric loss is decreasing. Over the higher frequency range, the increase in dielectric loss may be because of the loss due to the orientation of some dipoles that were inactive over lower frequency but becomes active over the higher frequency range. The dielectric loss also increases as the loading of nanosilica increases. The addition of nano silica may be considered as nanodipoles/nanocapacitors.[26] Increasing the amount of nanosilica within the polymer matrix thus increases the number of such nanodipoles/nanocapacitors. As a result, the interface polarization as well as the orientation toward the direction of applied fields are increased. This is accounted for by the loss of electrical energy, and hence, the dielectric loss value is increased.

The Nyquist plots (cole−cole plots) of real and imaginary parts of the electrical modulus of the nanocomposites are presented in Figure 9c. These give an idea about the presence of any electrical polarization and relaxation process within the nanocomposite systems. The complex electric modulus (M^*) is related to the dielectric constant (ε') and loss (ε''), and the real (M') and imaginary (M'') parts of electric modulus as follows:[28,29]

$$M^* = \frac{1}{\varepsilon^*} = \frac{1}{\varepsilon' - i'\varepsilon''} = \frac{\varepsilon'}{\varepsilon'^2 + \varepsilon''^2} + i\frac{\varepsilon''}{\varepsilon'^2 + \varepsilon''^2} = M' + M'' \quad (2)$$

Two types of incomplete semicircles are observed from these cole−cole plots. The nature of the semicircle at a low value of M' is observed because of interface polarization between the interface of polymer matrices and nanosilica. However, distorted polarizations such as electronic and ionic are observed at a higher value of M' as is evident from their semicircle nature.[30] It is observed from the figure that the nature of the semicircle is more evident when the loading of nanosilica is increasing. This indicates that with the increase in the loading of nanosilica, the effects of all types of polarizations have increased marginally.

The dielectric breakdown strength (DBS) of the optimized blend and its uncured and cured nanocomposites are presented in Figure 10. It is observed that the breakdown strength has increased up to a certain loading of composite (M3 composite) and then declined for its highest loading of composite (M5). There is an approximate 37% increment in breakdown strength for the M3 composite compared to the M0 one. This increment can be attributed to the barrier effect of nanosilica, which in turn increases the tree propagation time of the fire and thus results in the high value of dielectric breakdown strength.[28,31] The increase in nanosilica loading may have created defects, voids, cracks, or agglomeration within the

https://doi.org/10.1021/acsomega.3c06766
ACS Omega 2024, 9, 828−836

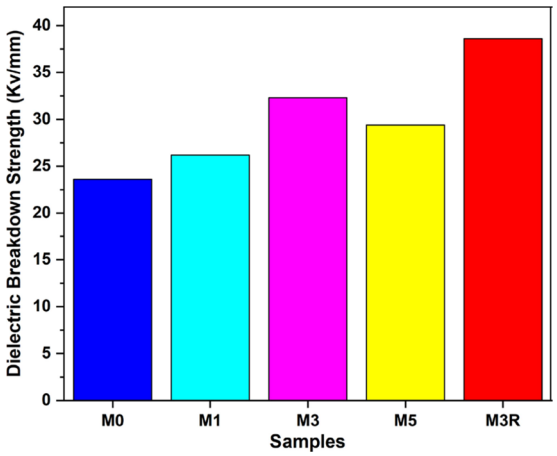

Figure 10. Dielectric breakdown strength of nanosilica-filled nanocomposites.

composite M5 and thus the breakdown strength has been reduced. We have observed the breakdown strength increment for the radiation-cured composite (M3R). The result shows that there is an approximate 63.6% increment in the DBS value for the M3R composite compared to the M0 composite. This can be attributed to the curing of the matrix. This creates networks of chemical bonding within the polymer chains. Hence, there is the need for extra electrical energy to breakdown these bonds: as a result, the time for tree propagation is increased, and this is why the breakdown strength value is increased.

4. CONCLUSIONS

A novel blend system based on LLDPE and PDMS was successfully prepared, and necessary tests were performed for its proposed application in outdoor high-voltage transmission power cable lines as well as in indoor power cable jackets as an insulating compound. The irradiation reduced the melting temperature and crystallinity of the base polymers as well as their blend. However, in the blend system, the melting points corresponding to PDMS have shifted to higher values. The thermal stability improved after irradiation of the blend, and a radiation dose of 100 kGy was found to be more effective in this case. When considering the nanosilica loading, 3 wt % loaded nanocomposites and their irradiated sample showed better thermal stability. There is a 15 °C improvement in thermal stability for the M3 composite compared to its base blend (LL50) due to the combined effect of irradiation and nanosilica loading. Moreover, the nanosilica loading has improved the dielectric constant and loss and dielectric breakdown strength values. The dielectric breakdown strength was observed better for the M3 nanocomposite. This showed an improvement of 37%. It further improved to 63.6% after irradiation of the sample. This is because of the curing of the sample that makes internal networks and thereby absorbs more energy for its complete failure. The M3R nanocomposite has resulted in a dielectric breakdown strength value of 38 kV/mm. Overall, it is observed that there is substantial improvement in thermal stability, dielectric constant value, and dielectric breakdown strength value for the optimum nanocomposite. The highest-loaded nanocomposite (M5) showed a 26.7% decrease in DC electrical resistivity. Moreover, the M3R nanocomposite exhibited the lowest value of electrical resistivity. The highest value is observed for the M0 blend. This has been attributed to the polarity of the silanol group of nanosilica and the compactness of nanosilica particles because of curing, which facilitates the mobility of charge carriers and consequently reduces electrical resistivity. Though the M0 blend is more insulating compared to the M3R nanocomposite, it is the dielectric breakdown strength value, which governs its applicability for high-voltage cable insulation. The result of the dielectric breakdown strength value implies that the M3R nanocomposite is highly suitable as a jacket for outdoor and indoor power cables.

AUTHOR INFORMATION

Corresponding Author

Radhashyam Giri − *Department of Plastics Technology, CIPET: Institute of Petrochemicals Technology, Chennai, Tamilnadu 600032, India;* orcid.org/0009-0003-9031-4387; Email: giripolymer@gmail.com

Authors

Mostafizur Rahaman − *Department of Chemistry, College of Science, King Saud University, Riyadh 11451, Saudi Arabia;* orcid.org/0000-0002-5495-1771

Bibhudatta Paikaray − *Department of Electrical Engineering, GITA Autonomous College, Bhubaneswar, Odisha 752054, India*

Mobasserul Islam − *Department of Manufacturing Engineering, School of Mechanical Engineering, Vellore Institute of Technology, Vellore 632014, India*

Subhadip Mondal − *Department of Polymer-Nano Science and Technology, Jeonbuk National University, Jeonju 54896, South Korea;* orcid.org/0000-0001-5578-4621

Jayakrushna Moharana − *Department of Electrical Engineering, HIT, Bhubaneswar, Odisha 752057, India*

Saravanan Pandiaraj − *Department of Physics, College of Science, King Saud University, Riyadh 11451, Saudi Arabia*

Govindasami Periyasami − *Department of Chemistry, College of Science, King Saud University, Riyadh 11451, Saudi Arabia;* orcid.org/0000-0003-1181-1645

Complete contact information is available at: https://pubs.acs.org/10.1021/acsomega.3c06766

Notes

The authors declare no competing financial interest.

ACKNOWLEDGMENTS

The authors acknowledge the Researchers Supporting Project number (RSPD2023R674), King Saud University, Riyadh, Saudi Arabia for funding this research work.

REFERENCES

(1) Miranda, I.; Souza, A.; Sousa, P.; Ribeiro, J.; Castanheira, E. M.; Lima, R.; Minas, G. Properties and applications of PDMS for biomedical engineering: A review. *Journal of functional biomaterials* **2022**, *13* (1), 2.

(2) (a) Fujii, T. PDMS-based microfluidic devices for biomedical applications. *Microelectronic engineering* **2002**, *61*, 907−914. (b) Zhou, J.; Ellis, A. V.; Voelcker, N. H. Recent developments in PDMS surface modification for microfluidic devices. *Electrophoresis* **2010**, *31* (1), 2−16.

(3) Kumar, R.; Sahani, A. K. Role of superhydrophobic coatings in biomedical applications. *Mater. Today: Proc.* **2021**, *45*, 5655−5659.

(4) Kim, S.-J.; Lee, D.-S.; Kim, I.-G.; Sohn, D.-W.; Park, J.-Y.; Choi, B.-K.; Kim, S.-W. Evaluation of the biocompatibility of a coating

https://doi.org/10.1021/acsomega.3c06766
ACS Omega 2024, 9, 828−836

material for an implantable bladder volume sensor. *Kaohsiung journal of medical sciences* **2012**, *28* (3), 123−129.
(5) Wu, X.; Kim, S.-H.; Ji, C.-H.; Allen, M. G. A solid hydraulically amplified piezoelectric microvalve. *Journal of Micromechanics and Microengineering* **2011**, *21* (9), No. 095003.
(6) Doutel, E.; Viriato, N.; Carneiro, J.; Campos, J. B.; Miranda, J. M. Geometrical effects in the hemodynamics of stenotic and non-stenotic left coronary arteries—numerical and in vitro approaches. *Int. J. Numer. Methods Biomed. Eng.* **2019**, *35* (8), No. e3207.
(7) Chen, W.; Lam, R. H.; Fu, J. Photolithographic surface micromachining of polydimethylsiloxane (PDMS). *Lab Chip* **2012**, *12* (2), 391−395.
(8) Schneider, F.; Fellner, T.; Wilde, J.; Wallrabe, U. Mechanical properties of silicones for MEMS. *Journal of Micromechanics and Microengineering* **2008**, *18* (6), No. 065008.
(9) Zhang, H.; Cai, C.; Liu, W.; Li, D.; Zhang, J.; Zhao, N.; Xu, J. Recyclable polydimethylsiloxane network crosslinked by dynamic transesterification reaction. *Sci. Rep.* **2017**, *7* (1), 11833.
(10) Singh, P.; Venugopal, B.; Nandini, D. Effect of electron beam irradiation on polymers. *Journal of Modern Materials* **2017**, *5* (1), 24−33.
(11) Nielsen, L. E. Cross-linking−effect on physical properties of polymers. *Journal of Macromolecular Science, Part C* **1969**, *3* (1), 69−103.
(12) (a) Clegg, D.; Collyer, A. A. *Irradiation effects on polymers*; 1991. (b) Giri, R.; Naskar, K.; Nando, G. B. Effect of electron beam irradiation on dynamic mechanical, thermal and morphological properties of LLDPE and PDMS rubber blends. *Radiation physics and chemistry* **2012**, *81* (12), 1930−1942.
(13) (a) Sharif, J.; Aziz, S. H. S. A.; Hashim, K. Radiation effects on LDPE/EVA blends. *Radiat. Phys. Chem.* **2000**, *58* (2), 191−195. (b) Mateev, M.; Karageorgiev, S. Radiation-induced transformation of polypropylene morphology and visco-elastic behaviour. *Radiation effects and defects in solids* **2000**, *152* (2), 109−138.
(14) Ratnam, C. T.; Kamaruddin, S.; Sivachalam, Y.; Talib, M.; Yahya, N. Radiation crosslinking of rubber phase in poly (vinyl chloride)/epoxidized natural rubber blend: Effect on mechanical properties. *Polym. Test.* **2006**, *25* (4), 475−480.
(15) Van gisbergen, J.; Meijer, H. Influence of electron beam irradiation on the microrheology of incompatible polymer blends: thread break-up and coalescence. *J. Rheol.* **1991**, *35* (1), 63−87.
(16) Satapathy, S.; Chattopadhyay, S.; Chakrabarty, K.; Nag, A.; Tiwari, K.; Tikku, V.; Nando, G. Studies on the effect of electron beam irradiation on waste polyethylene and its blends with virgin polyethylene. *J. Appl. Polym. Sci.* **2006**, *101* (1), 715−726.
(17) (a) Giri, R.; Naskar, K.; Nando, G. B. In-situ compatibilization of linear low-density polyethylene and Polydimethyl siloxane rubber through reactive blending. *Materials Express* **2012**, *2* (1), 37−50. (b) Giri, R.; Sureshkumar, M.; Naskar, K.; Bharadwaj, Y.; Sarma, K.; Sabharwal, S.; Nando, G. Electron beam irradiation of LLDPE and PDMS rubber blends: studies on the physicomechanical properties. *Advances in Polymer Technology: Journal of the Polymer Processing Institute* **2008**, *27* (2), 98−107. (c) Giri, R.; Naskar, K.; Nando, G. Effect of electron beam irradiation on the structure property relationship of LLDPE and PDMS rubber blends. *Rubber Fibres Plast. Int.* **2011**, *6*, 97−107.
(18) Hidayah, I.; Mariatti, M.; Ismail, H.; Kamarol, M. Effect of selective localization on dielectric properties of boron nitride nanofiller filled linear low density polyethylene (LLDPE)/silicone rubber (SR) blends. *Polym. Test.* **2016**, *56*, 131−139.
(19) Said, A.; Abd-allah, M.; Nawar, A. G.; Elsayed, A. E.; Kamel, S. Enhancing the electrical and physical nature of high-voltage XLPE cable dielectric using different nanoparticles. *Journal of Materials Science: Materials in Electronics* **2022**, *33* (10), 7435−7443.
(20) (a) Yu, S.; Lee, S. H.; Han, J. A.; Ahn, M. S.; Park, H.; Han, S. W.; Lee, D. H. Insulative ethylene-propylene copolymer-nano-structured polypropylene for high-voltage cable insulation applications. *Polymer* **2020**, *202*, No. 122674. (b) Thomas, J.; Joseph, B.; Jose, J. P.; Maria, H. J.; Main, P.; Ali rahman, A.; Francis, B.; Ahmad, Z.; Thomas, S. Recent advances in cross-linked polyethylene-based nanocomposites for high voltage engineering applications: a critical review. *Ind. Eng. Chem. Res.* **2019**, *58* (46), 20863−20879. (c) Andritsch, T.; Vaughan, A.; Stevens, G. C. Novel insulation materials for high voltage cable systems. *IEEE Electrical Insulation Magazine* **2017**, *33* (4), 27−33. (d) Huang, X.; Sun, B.; Yu, C.; Wu, J.; Zhang, J.; Jiang, P. Highly conductive polymer nanocomposites for emerging high voltage power cable shields: experiment, simulation and applications. *High Voltage* **2020**, *5* (4), 387−396. (e) Hosier, I. L.; Vaughan, A. S.; Swingler, S. G. An investigation of the potential of ethylene vinyl acetate/polyethylene blends for use in recyclable high voltage cable insulation systems. *J. Mater. Sci.* **2010**, *45*, 2747−2759.
(21) (a) Charlesby, A.; Pinner, S. Analysis of the solubility behaviour of irradiated polyethylene and other polymers. *Proc. R. Soc. Lond., Ser. A: Math. Phys. Sci.* **1959**, *249* (1258), 367−386. (b) Greer, R. W.; Wilkes, G. L. Apparent reversal of physical aging by electron beam irradiation—further investigations. *Polymer* **1998**, *39* (18), 4205−4210.
(22) (a) Li, Y.; Han, B.; Wen, S.; Lu, Y.; Yang, H.; Zhang, L.; Liu, L. Effect of the temperature on surface modification of silica and properties of modified silica filled rubber composites. *Composites Part A: Applied Science and Manufacturing* **2014**, *62*, 52−59. (b) Sae-oui, P.; Sirisinha, C.; Hatthapanit, K.; Thepsuwan, U. Comparison of reinforcing efficiency between Si-69 and Si-264 in an efficient vulcanization system. *Polym. Test.* **2005**, *24* (4), 439−446.
(23) Poplavko, Y.; Borisov, A. Polarization influence on conductivity. In *2017 IEEE 37th International Conference on Electronics and Nanotechnology (ELNANO)*; 2017; IEEE, pp 21−26.
(24) Rahaman, M.; Chaki, T. K.; Khastgir, D. Control of the temperature coefficient of the DC resistivity in polymer-based composites. *J. Mater. Sci.* **2013**, *48* (21), 7466−7475.
(25) Ismail, N. H.; Mustapha, M.; Ismail, H.; Jamil, M. K.; Hairaldin, S. Z. Effect of electron beam irradiation on dielectric properties, morphology and melt rheology of linear low density polyethylene/silicone rubber-based thermoplastic elastomer nanocomposites. *Polym. Eng. Sci.* **2018**, *58* (S1), E135−E144.
(26) Rahaman, M.; Thomas, S. P.; Hussein, I. A.; De, S. Dependence of electrical properties of polyethylene nanocomposites on aspect ratio of carbon nanotubes. *Polym. Compos.* **2013**, *34* (4), 494−499.
(27) Ram, R.; Rahaman, M.; Khastgir, D. Mechanical, electrical, and dielectric properties of polyvinylidene fluoride/short carbon fiber composites with low-electrical percolation threshold. *J. Appl. Polym. Sci.* **2014**, *131*, 39866.
(28) Islam, M.; Rahaman, M.; Aldalbahi, A.; Paikaray, B.; Moharana, J.; Mondal, S.; Das, N. C.; Gupta, P.; Giri, R. High density polyethylene and metal oxides based nanocomposites for high voltage cable application. *J. Appl. Polym. Sci.* **2022**, *139* (11), 51787.
(29) Ignaczak, W.; Ladegaard skov, A.; El fray, M. Interfacial polarization in thermoplastic basalt fiber-reinforced composites. *Polymers* **2020**, *12* (7), 1486.
(30) Gaabour, L. Study of the structural, AC electrical conductivity, electric modulus, and dielectric properties of novel PVDF/LiCoO2 nanocomposites for Li-ion batteries. *AIP Adv.* **2021**, *11* (9), No. 095114.
(31) Hamzah, M. S.; Jaafar, M.; Mohd Jamil, M. K. Electrical insulation characteristics of alumina, titania, and organoclay nano-particles filled PP/EPDM nanocomposites. *J. Appl. Polym. Sci.* **2014**, *131* (23), 41184.

https://doi.org/10.1021/acsomega.3c06766
ACS Omega 2024, 9, 828−836